Supporting Information for

Stepwise structure evolution from 2D cluster-based frameworks to silver(I) clusters

Qiu-Xu Zang,[a] Zhao-Yang Wang,[a] Yao Li,[a] Xi-Ming Luo,[a] Hai-Yang Li,[a] Ya-Nan Si*[a] & Shuang-Quan Zang*[a]

[a]*Henan Key Laboratory of Crystalline Molecular Functional Materials, Henan International Joint Laboratory of Tumor Theranostical Cluster Materials, Green Catalysis Center, and College of Chemistry, Zhengzhou University, Zhengzhou 450001, China*

* *E-mail address*: siyanan@zzu.edu.cn; zangsqzg@zzu.edu.cn

Table of Contents

Scheme S1. Synthetic route of *R*-L

Figure S1. ^{1}H NMR spectrum of compound *R*-AcS in $CDCl_3$

Figure S2. ^{1}H NMR spectrum of compound *R*-L in $CDCl_3$

Scheme S2. Synthetic route of *S*-L

Figure S3. ^{1}H NMR spectrum of compound *S*-AcS in $CDCl_3$

Figure S4. ^{1}H NMR spectrum of compound *S*-L in $CDCl_3$

Figure S5. Packing of ***S*-Ag$_5$-1** in the crystal lattice

Figure S6. Triangular prism Ag_5S_6 in the host framework of ***R*-Ag$_5$-1** (left) and ***S*-Ag$_5$-1** (right) with mirror symmetry

Figure S7. Triangular biconical Ag_5 kernels of ***R*-Ag$_5$-1** (left) and ***S*-Ag$_5$-1** (right) in channels.

Figure S8. The coordination configurations of Na^+ in ***S*-Ag$_5$-1**.

Figure S9. From the *c*-axis, carbonyl groups on two of the three ligands in the upper layer of each triangular prism Ag_5S_6 node coordinate with Na^+ (azure), and only one Na^+ (purple) in the lower layer participates in the coordination

Figure S10. The PXRD of ***R*-Ag$_5$-1** and ***S*-Ag$_5$-1**

Table S1. ICP analysis of Ag and Na contents and calculated ratios in ***R*-Ag$_5$-1** and ***S*-Ag$_5$-1**

Figure S11. Packing of ***S*-Ag$_5$-2** in the crystal lattice at 200 K

Figure S12. Packing of ***S*-Ag$_5$-2** in the crystal lattice at 295 K

Figure S13. Considerable bond contractions of Ag–Ag bonds and Ag–S bonds in each tri-prism Ag_5S_6 node from 200 K to 295 K

Figure S14. Positive-ion mode ESI-MS of ***S*-Ag$_5$-3** and ***S*-Ag$_5$-3'** dissolved in CH_3OH

Figure S15. Packing of ***S*-Ag$_5$-3** in the crystal lattice

Figure S16. The Ag_5 clusters and triangular biconical Ag_5 kernels of ***R*-Ag$_5$-3** (left) and ***S*-Ag$_5$-3** (right) with mirror symmetry

Figure S17. TG curves of ***S*-Ag$_5$-3** and ***R*-Ag$_5$-3**

Figure S18. The UV-vis absorption spectra of ***R*-Ag$_5$-1** and ***R*-Ag$_5$-3** in solid state at RT

Figure S19. Decay lifetimes of ***R*-Ag$_5$-3** (a) and ***S*-Ag$_5$-3** (b) in solid state

Figure S20. Selected frontier molecular orbitals of ***R*-Ag$_5$-3'**.

Figure S21. Experimental optical absorption spectrum (black) of ***R*-Ag$_5$-3** in CH_3OH compared to the calculated spectrum (red)

Figure S22. Corresponding g_{lum} values of ***S*-Ag$_5$-3** (black curve) and ***R*-Ag$_5$-3** (red curve) in the solid state.

Table S2. Crystal data and structure refinements for ***R*-Ag$_5$-1** and ***S*-Ag$_5$-1** at 200 K

Table S3. Crystal data and structure refinements for ***R*-Ag$_5$-2** and ***S*-Ag$_5$-2** at 200 K

Table S4. Crystal data and structure refinements for ***R*-Ag$_5$-2** and ***S*-Ag$_5$-2** at 295 K

Table S5. Crystal data and structure refinements for ***R*-Ag$_5$-3'** and ***S*-Ag$_5$-3'** at 200 K

References

Materials and reagents.

All reagents and solvents used are commercially available reagent grade and require no further purification.

Instrumentation.

Powder X-ray diffraction (PXRD) pattern of the sample on the D/MAX-3D diffractometer. Thermogravimetric analysis (TGA) was performed on a TA Q50 system from room temperature (RT) to 800 °C under nitrogen atmosphere at a heating rate of 10 °C/min. Mass spectrum (MS) were obtained on an X500R QTOF spectrometer.

Crystallographic data collection and structural refinement.

Single-crystal X-ray diffraction measurements of ***R*-Ag_5-1, *S*-Ag_5-1, *R*-Ag_5-3'** and ***S*-Ag_5-3'** were performed on a Rigaku XtaLAB Pro diffractometer with Cu-Kα radiation (λ = 1.54184 A) at 200 K. Data collection and reduction were performed using the program CrysAlisPro[1,2]. Single-crystal X-ray diffraction measurements of ***R*-Ag_5-2** and ***S*-Ag_5-2** were performed on a Bruker D8 VENTURE diffractometer with Mo-Kα radiation (λ = 0.71073 Å) at 200 K and 295 K. Data reduction was performed using the APEX3 software package. All the structures were solved with direct methods (SHELXS)[3] and refined by full-matrix least-squares on F^2 using OLEX2[4], which utilizes the SHELXL2015 module[5]. All atoms are anisotropically refined, and the hydrogen atoms are placed at calculated positions in the ideal geometry and assigned fixed isotropic displacement parameters. Detailed information about the X-ray crystallography data, intensity collection procedure, and refinement results for all cluster compounds is summarized in Tables S1- S6. The data can be obtained free of charge from The Cambridge Crystallographic Data Centre via www.ccdc.cam.ac.uk/data_request/cif.

Photophysical measurements.

UV-visible absorption spectra were recorded in the range of 200-800 nm using a Hitachi UH4150 UV-visible spectrophotometer. Emission and excitation spectra at RT were recorded with a HORIBA FluoroLog-3 fluorescence spectrometer. The luminescence lifetimes were measured on a HORIBA FluoroLog-3 fluorescence spectrometer operating in time-correlated single-photon counting (TCSPC) mode. The photoluminescence quantum yield (PLQY) was measured using an integrating sphere on a HORIBA FluoroLog-3 fluorescence spectrometer. Circular dichroism (CD) spectra were measured on a Chirascan V100 spectropolarimeter. Circularly polarized luminescence (CPL) spectra were measured on a JASCO CPL-300 spectrometer.

Quantum chemical calculations.

Density functional theory (DFT) calculations were performed with Gaussian 16[6] with the Perdew–Burke–Ernzerhof (PBE) exchange-correlation functional[7] using the 6-31g* basis set for the H, C and N atoms[8-9] and SDD effective core potentials for the Ag atoms[10]. The single-crystal structure of ***R/S*-Ag_5-1** was chosen as the initial guess

for the ground state optimization and all reported stationary points were verified as true minima by the absence of negative eigenvalues in the vibrational frequency analysis. The calculated absorption spectra were derived from GaussSum 2.1[11]. Hirshfeld population analysis was obtained by Multiwfn 3.4.1[12].

Synthesis of the chiral *R*-*tert*-Butyl-3-Mercaptopyrrolidine-1-carboxylate (*R*-L).

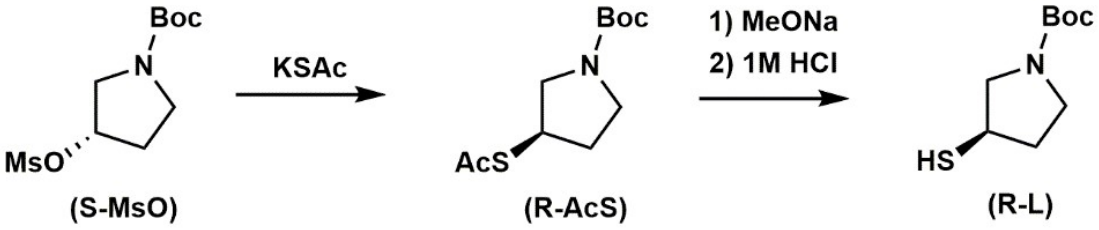

Scheme S1. Synthetic route of *R*-L.

Synthesis of *R*-*tert*-Butyl-3-(acetylsulfanyl)pyrrolidine-1-carboxylate(*R*-AcS). Under atmospheric atmosphere, *S*-*tert*-Butyl-3-((methylsulfonyl)oxy)pyrrolidine-1-carboxylate (*S*-MsO, 1.32 g, 5 mmol), potassium thioacetate (1.14 g, 10 mmol), and acetone solution (80 mL) were added sequentially in a 100 mL round-bottom flask. The mixture was reacted at reflux for 20 h at 60 °C. After the reaction, the solution was cooled to room temperature. The precipitate was removed by filtration and discarded. The filtrate was concentrated under reduced pressure and the residue was purified by flash column chromatography (silica gel; eluent, hexanes/ethyl acetate (8:1 (v/v)) to give a tan oil. 1H NMR ($CDCl_3$，600 MHz)：δ = 3.94-3.74 (dd，2H)，3.75 (dd，1H)，3.41-3.23 (m，3H)，2.32 (s，3H)，2.29 (dd，1H)，1.86 (dd，1H)，1.45 (s，9H).

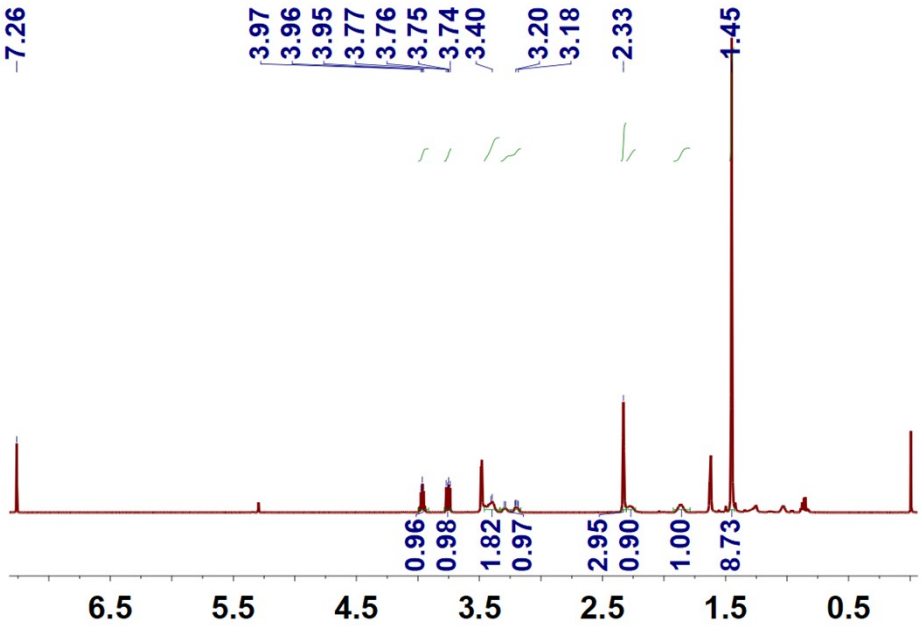

Figure S1. ^{1}H NMR spectrum of compound *R*-AcS in $CDCl_3$.

Under atmospheric atmosphere, *R*-AcS (1.4 g, 5 mmol), methanol solution (30 mL) were added sequentially in a 100 mL round-bottom flask. After stirring well, the mixture was cooled to 0°C in an ice bath. Sodium methoxide (0.61 g, 11.3 mmol) was then added to the round bottom flask. The reaction was then returned to room temperature and allowed to react at room temperature for 6 hours. After the reaction was completed, 1 M HCl was added to the round bottom flask for neutralization. The solution was then rotary evaporated and the product was concentrated. The reaction mixture was diluted with ethyl acetate (250ml) and a brine solution (250 ml) was added. The mixture was extracted with ethyl acetate three times and dried over anhydrous $MgSO_4$. The solution was evaporated to dryness, and the residue was purified by column chromatography on silica gel using hexanes/ethyl acetate (6:1, v/v) as eluent to offer a colorless oil. 1H NMR (CDCl3，600 MHz)：δ = 3.73 (d，1H)，3.54 (d，1H)，3.39 (s，2H)，3.20 (d，1H)，2.27 (td，1H)，1.82 (s，1H)，1.69 (d，1H)，1.46 (s，9H).

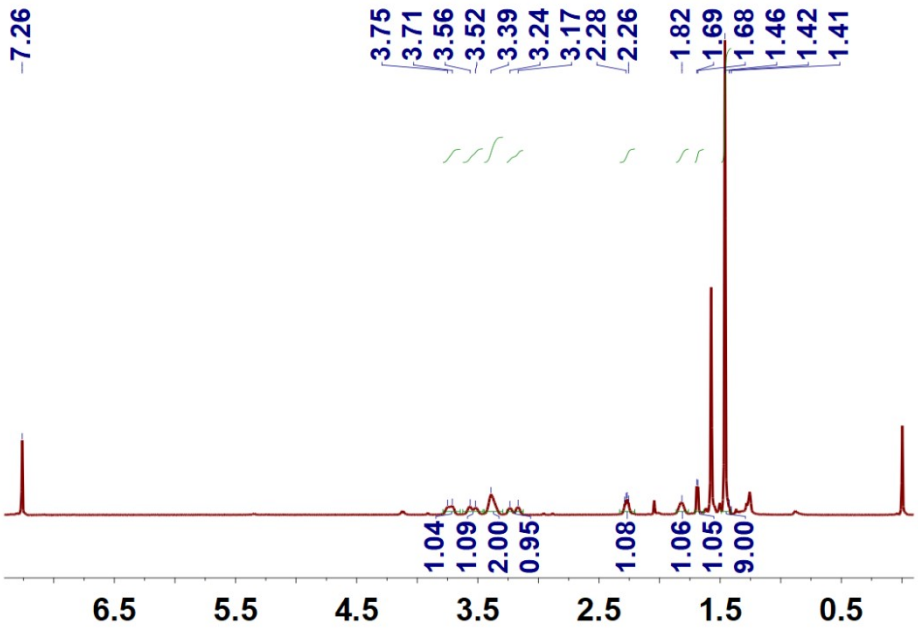

Figure S2. ^{1}H NMR spectrum of compound *R*-L in $CDCl_3$.

Synthesis of the chiral S-*tert*-Butyl-3-Mercaptopyrrolidine-1-carboxylate (*S*-L).

Scheme S2. Synthetic route of *S*-L.

The synthesis was the same as that of *R*-L ligand with the exception of the use of *R*-*tert*-Butyl-3-((methylsulfonyl)oxy)pyrrolidine-1-carboxylate in place of *S*-*tert*-Butyl-3-((methylsulfonyl)oxy)pyrrolidine-1-carboxylate.

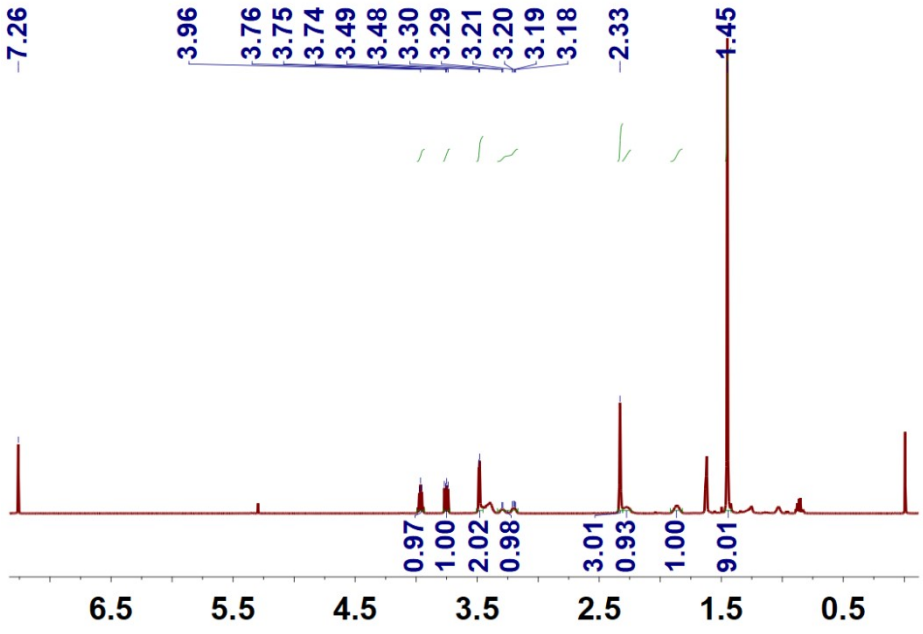

Figure S3. ^{1}H NMR spectrum of compound *S*-AcS in $CDCl_3$.

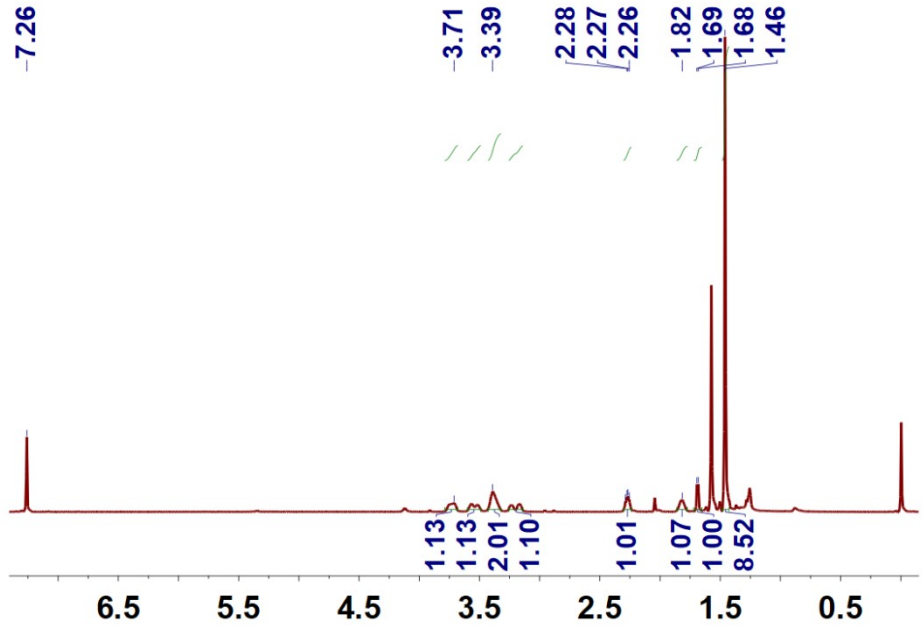

Figure S4. ^{1}H NMR spectrum of compound *S*-L in $CDCl_3$.

Synthesis of enantiomers *R/S*-Ag_5-1, *R/S*-Ag_5-2, and *R/S*-Ag_5-3' single crystals.

***R*-Ag_5-1 and *S*-Ag_5-1:** The chiral *R*-L (or *S*-L) (5 μL, 0.025 mmol) and $AgNO_3$ (4.2 mg,0.025 mmol) were dissolved in a mixture of 2 mL CH_3OH and 2 mL CH_3CN. The solution was vigorously stirred (1000 rpm) with magnetic stirring for 10 min. Then, 1 mL $NaBH_4$ methanol solution (5 mg mL^{-1}) was added quickly to the above reaction. The reaction was allowed to proceed for 12 h. After the reaction, the colorless supernatant was obtained by centrifugation. The colorless supernatant was evaporated away from light for 5 days to obtain colorless hexagonal massive crystals ***R*-Ag_5-1** (or ***S*-Ag_5-1)**. The crystals were filtered and washed with methanol with a yield of 31.3% (based on Ag).

***R*-Ag_5-3 and *S*-Ag_5-3:** The sample of ***R*-Ag_5-1** (or ***S*-Ag_5-1)** can be completely converted into ***R*-Ag_5-3** (or ***S*-Ag_5-3)** by leaving it in the air for several hours until the solvent molecules evaporated completely.

***R*-Ag_5-2 and *S*-Ag_5-2:** The undried crystals of ***R*-Ag_5-1** (or ***S*-Ag_5-1**) were soaked in anhydrous methanol for one week, and then corresponding crystals ***R*-Ag_5-2** (or ***S*-Ag_5-2**) with high quality were obtained.

In suit analysis: In order to determine the crystal structures of the intermediates ***R*-Ag_5-2** and ***S*-Ag_5-2**, the single crystal **Ag_5-1** was firstly heated in situ on a single crystal instrument at a heating rate of 10 ^oC min^{-1}. SCXRD analysis of **Ag_5-2** showed that the stacking patterns of the Ag_5 cluster-based unites in the intermediate crystal structure is still consistent with that of Ag_5-1, but sodium ions are out of the framework. Unfortunately, there were some disorders in the structure that caused irreparable errors (alert level B and level C) in the CheckCIF report due to fragmentation of the crystal, so the crystal structure of the intermediate that obtained by heating in suit cannot be used for publication. According to the coordination principle, we guessed that it was possible to cultivate single crystal with excellent quality by using protic solvent to compete for coordination with carbonyl group. Therefore, we soaked crystal ***R*-Ag_5-1** or ***S*-Ag_5-1** in anhydrous methanol for one week and found that the crystal parameters were consistent with those measured by in-situ heating method. The SCXRD analysis showed that we have indeed obtained an excellent intermediate crystal structure.

***R*-Ag_5-3'** and ***S*-Ag_5-3':** The chiral *R*-L (or *S*-L) (5 μL, 0.025 mmol) and $AgNO_3$ (4.2 mg, 0.025 mmol) were dissolved in a mixture of 2 mL CH_3OH and 2 mL CH_3CN. The solution was vigorously stirred (1000 rpm) with magnetic stirring for 10 min. Then, hydrazine hydrate (5 μL) was added quickly to the above reaction. The reaction was allowed to proceed for 12 h. After the reaction, the colorless supernatant was obtained by centrifugation. The colorless supernatant was evaporated away from light for about 5 days to obtain colorless hexagonal massive crystals. The crystals ***R*-Ag_5-3'** (or ***S*-Ag_5-3'**) were filtered and washed with methanol with a yield of 20.4% (based on Ag).

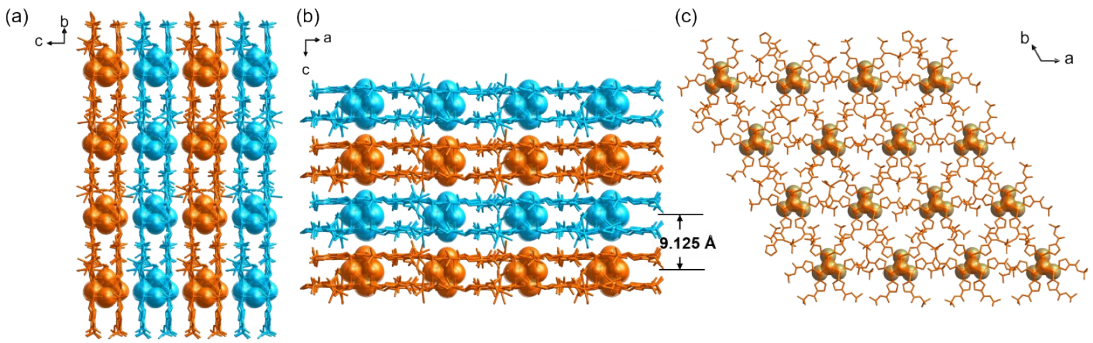

Figure S5. Packing of ***S*-Ag$_5$-1** in the crystal lattice: view from the *a*-axis (a), *b*-axis (b) and *c*-axis (c). Hydrogen atoms are omitted for clarity.

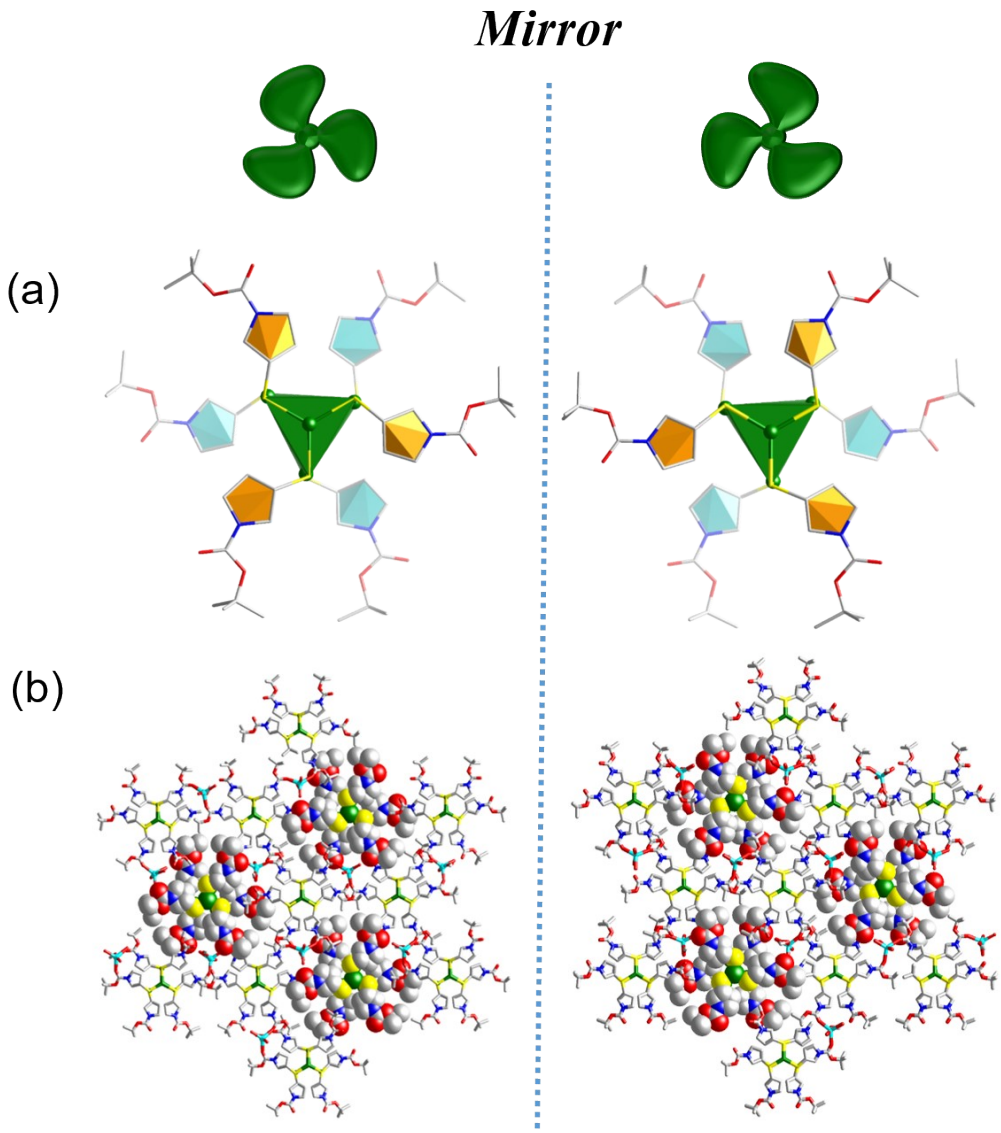

Figure S6. Structure introduction of ***R*-Ag$_5$-1** and ***S*-Ag$_5$-1** with mirror symmetry. (a) The Ag_5 cluster-based units of ***R*-Ag$_5$-1** (left) and ***S*-Ag$_5$-1** (right); (b) The 2D laminar structure of ***R*-Ag$_5$-1** (left) and ***S*-Ag$_5$-1** (right) with ordered chiral Ag_5 clusters in the channels viewed along the *c*-axis.

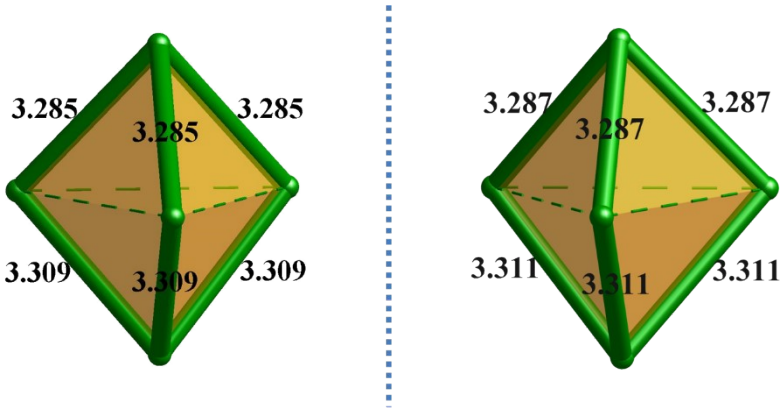

Figure S7. Triangular biconical Ag_5 kernels of ***R*-Ag$_5$-1** (left) and ***S*-Ag$_5$-1** (right) in channels.

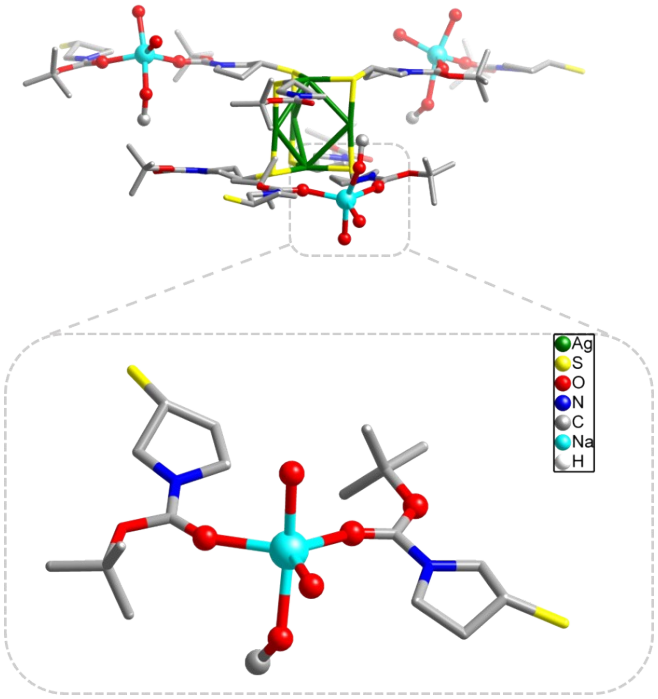

Figure S8. The coordination configurations of Na^+ in ***R*-Ag$_5$-1**. Hydrogen atoms are omitted for clarity.

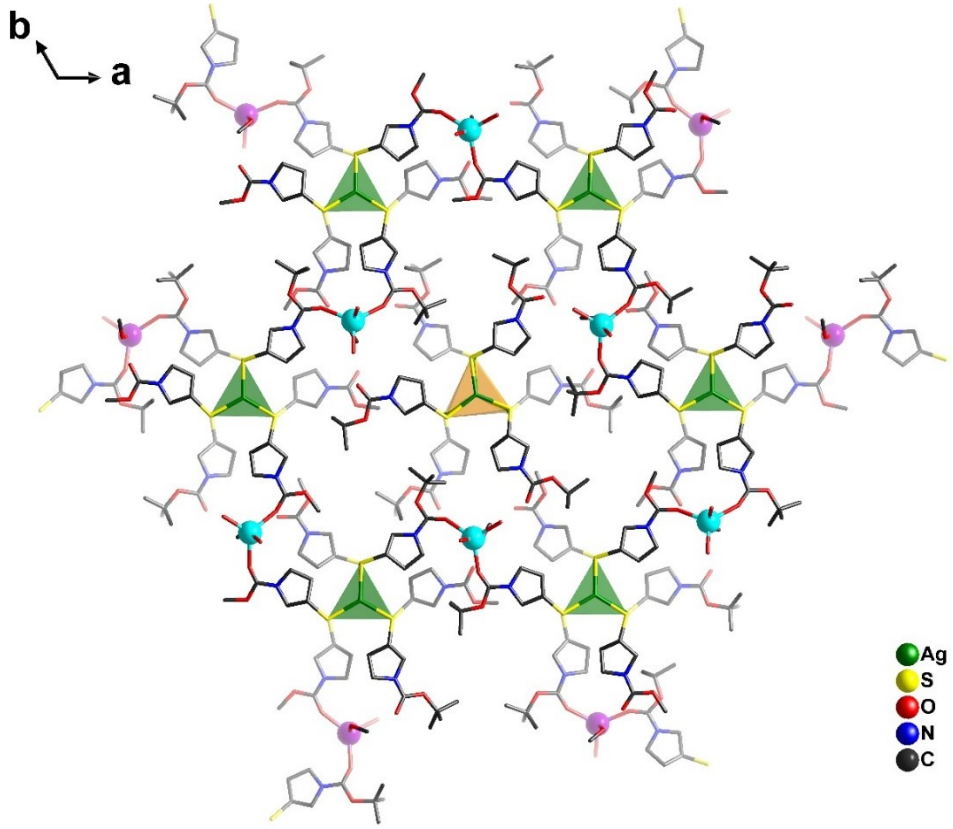

Figure S9. From the *c*-axis, carbonyl groups on two of the three ligands in the upper layer of each triangular prism Ag_5S_6 node coordinate with Na^+ (azure), and only one Na^+ (purple) in the lower layer participates in the coordination.

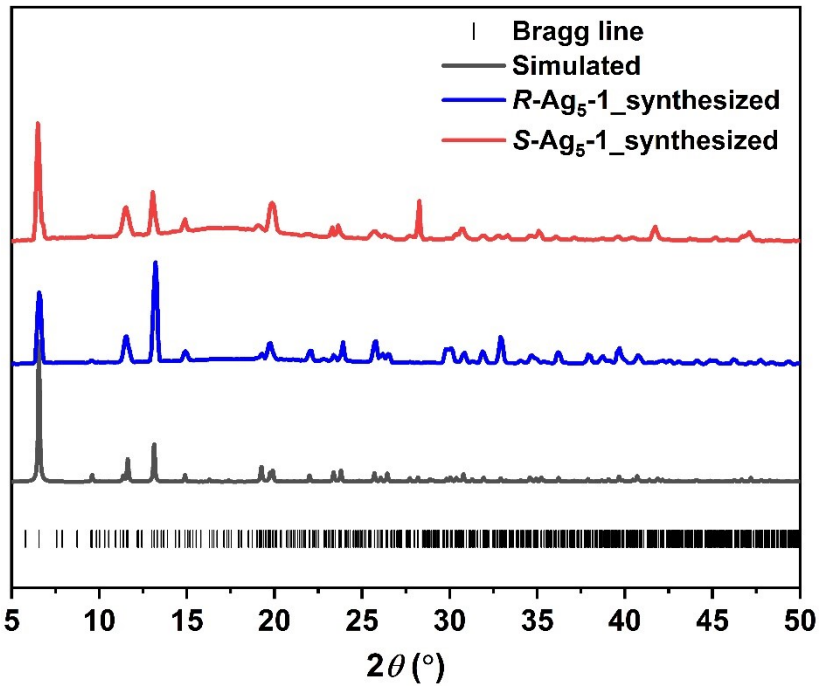

Figure S10. The PXRD of ***R*-Ag$_5$-1** and ***S*-Ag$_5$-1**. The phase purity of **Ag$_5$-1** was further confirmed via its powder X-ray diffraction (PXRD) spectrum.

Table S1. ICP analysis of Ag and Na contents and calculated ratios in ***R*- Ag$_5$-1** and ***S*-Ag$_5$-1.**

	Ag (ppm)		Na (ppm)	Ag : Na (mole ratio)
***R*-Ag$_5$-1**	17.49		3.94	4.5:1
***S*-Ag$_5$-1**	17.13		3.84	4.5:1

The results of inductively coupled plasma (ICP) analysis verified the silver-to-sodium ratio of the sample, which agreed with the results of the crystal-structure determination.

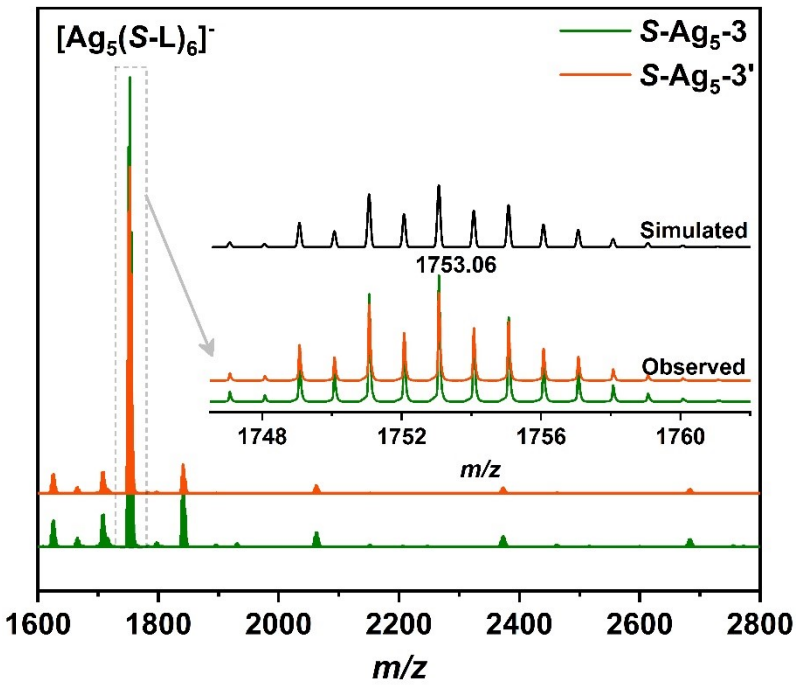

Figure S11. Positive-ion mode ESI-MS of ***S*-Ag$_5$-3** and ***S*-Ag$_5$-3'** dissolved in CH_3OH. Insets: Enlarged portion of the spectra showing the observed and simulated isotopic distribution patterns.

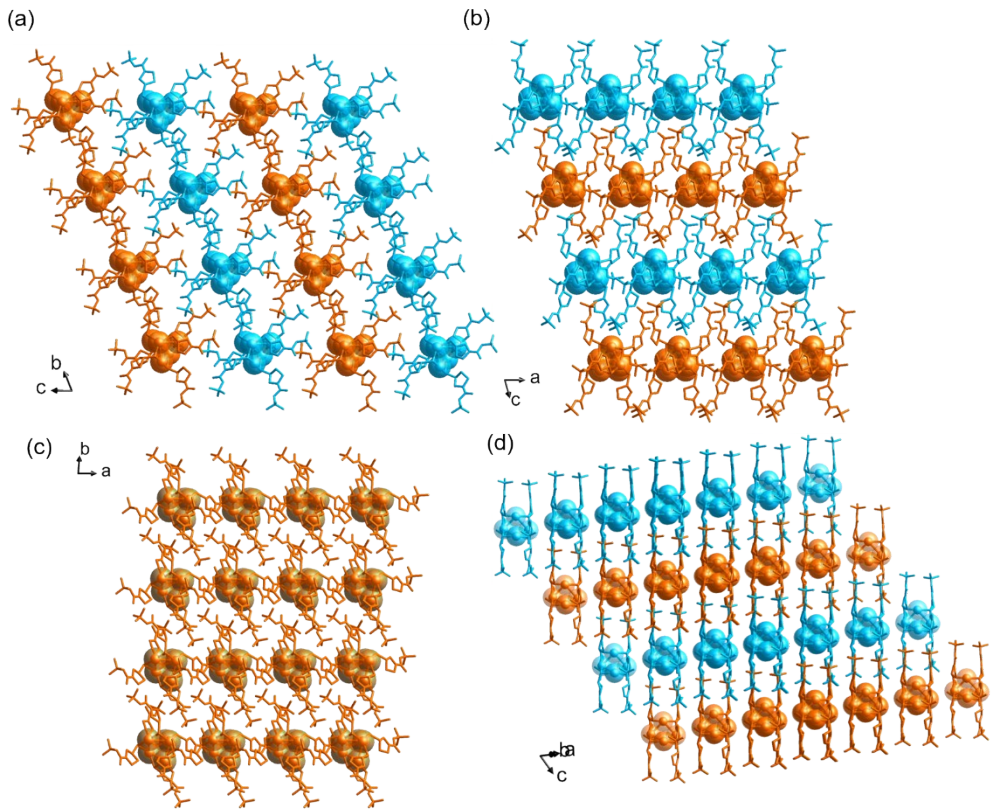

Figure S12. Packing of ***S*-Ag$_5$-3** in the crystal lattice. View from different axis. Hydrogen atoms are omitted for clarity.

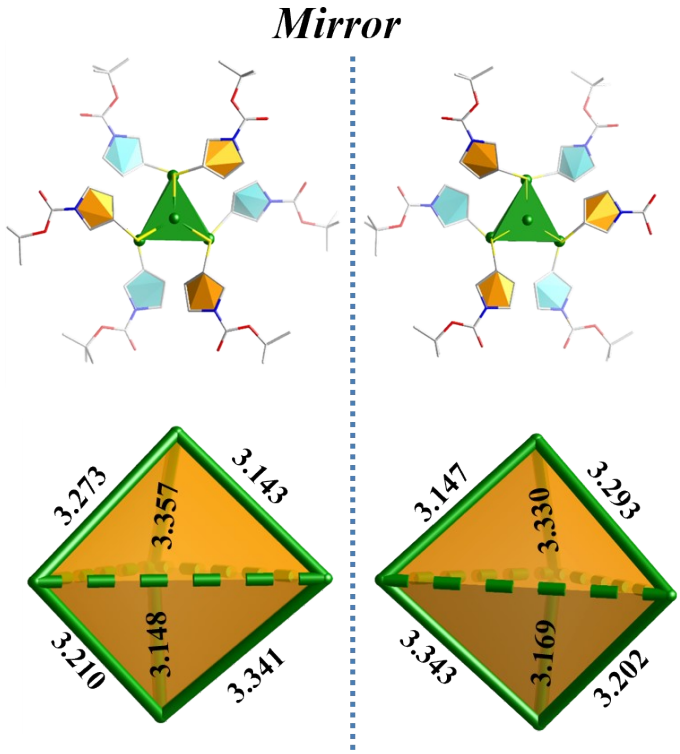

Figure S13. The Ag$_5$ clusters and triangular biconical Ag$_5$ kernels of ***R*-Ag$_5$-3** (left) and ***S*-Ag$_5$-3** (right) with mirror symmetry.

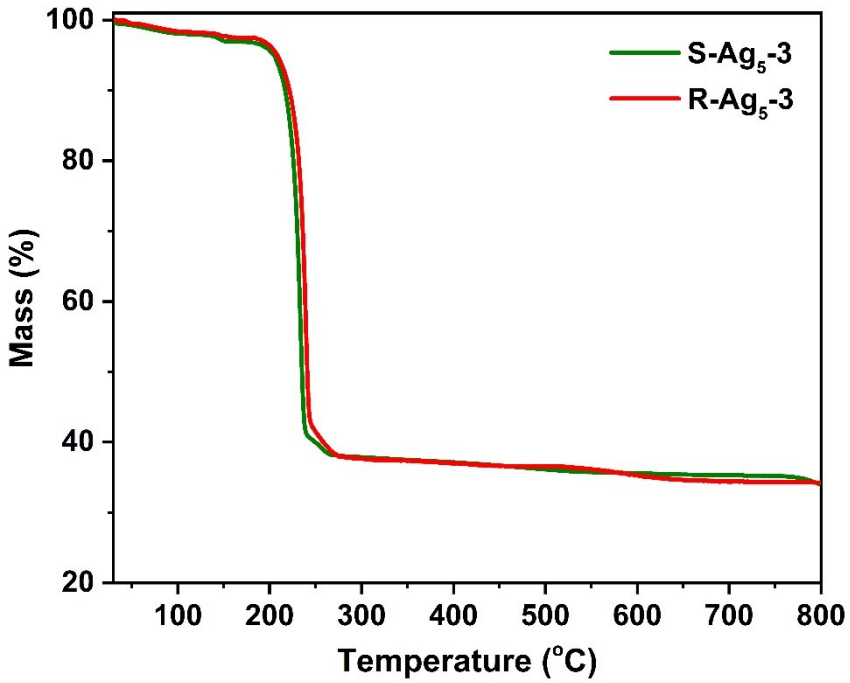

Figure S14. TG curves of ***S*-Ag$_5$-3** and ***R*-Ag$_5$-3**.

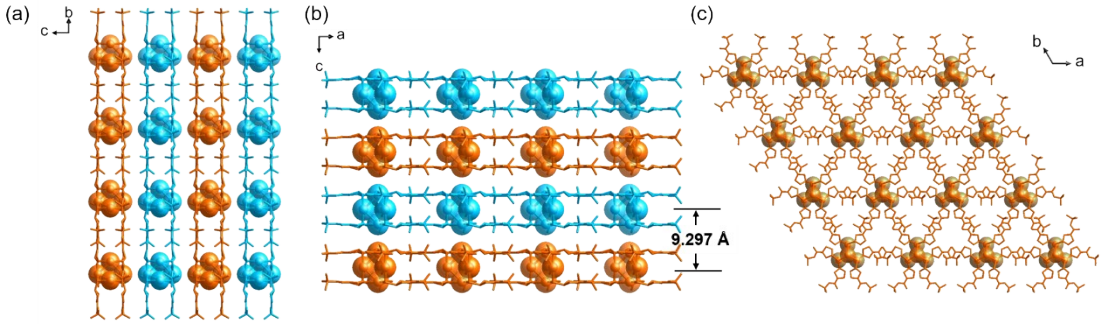

Figure S15. Packing of ***S*-Ag$_5$-2** in the crystal lattice at 200 K: view from the *a* axis (a), *b* axis (b) and *c* axis (c). Hydrogen atoms are omitted for clarity.

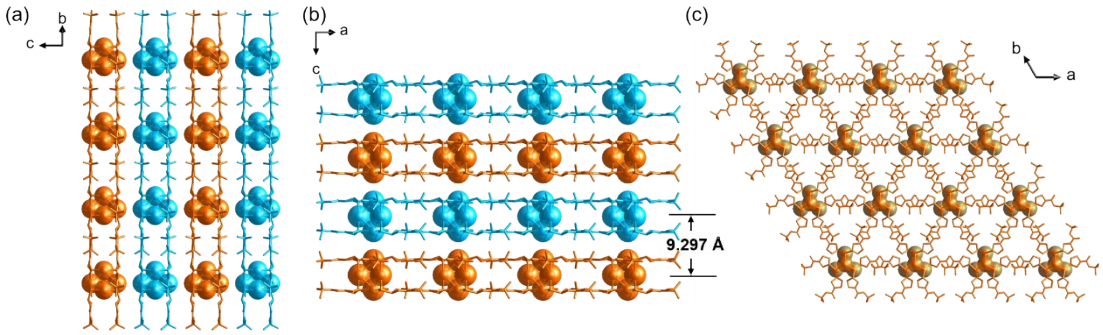

Figure S16. Packing of ***S*-Ag$_5$-2** in the crystal lattice at 295 K: view from the *a* axis (a), *b* axis (b) and *c* axis (c). Hydrogen atoms are omitted for clarity.

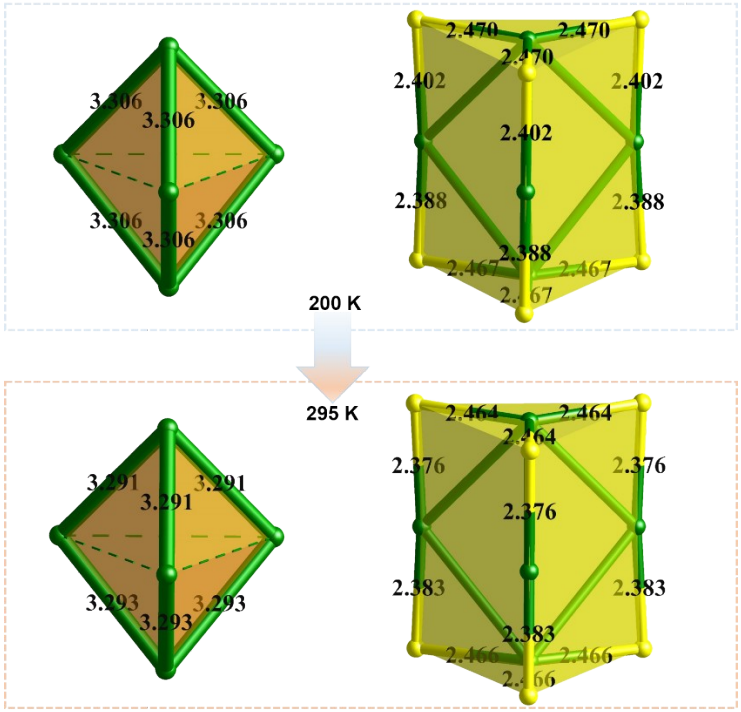

Figure S17. Considerable bond contractions of Ag–Ag bonds and Ag–S bonds in each tri-prism Ag_5S_6 node from 200 K to 295 K.

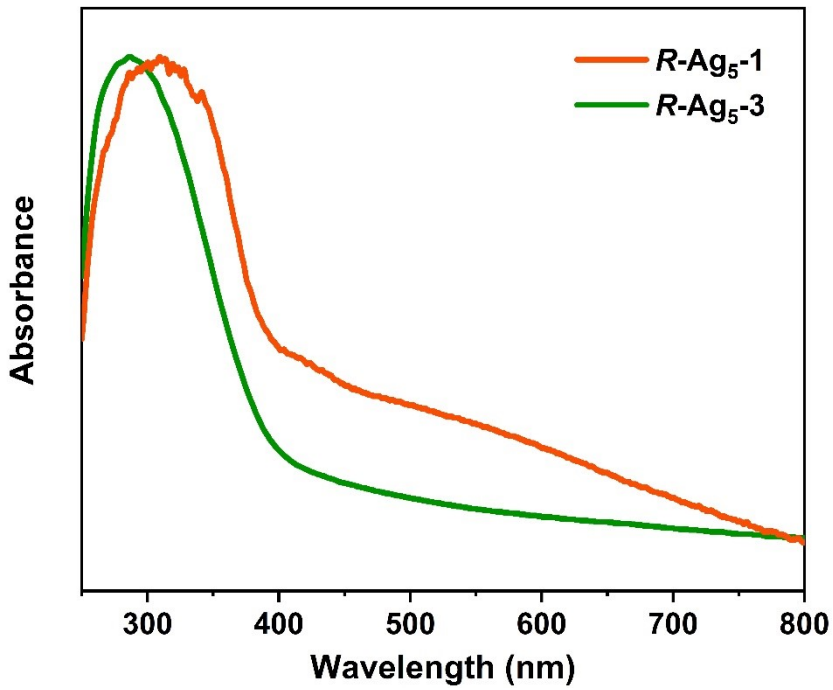

Figure S18. The UV-vis absorption spectra of ***R*-Ag$_5$-1** and ***R*-Ag$_5$-3** in solid state at RT.

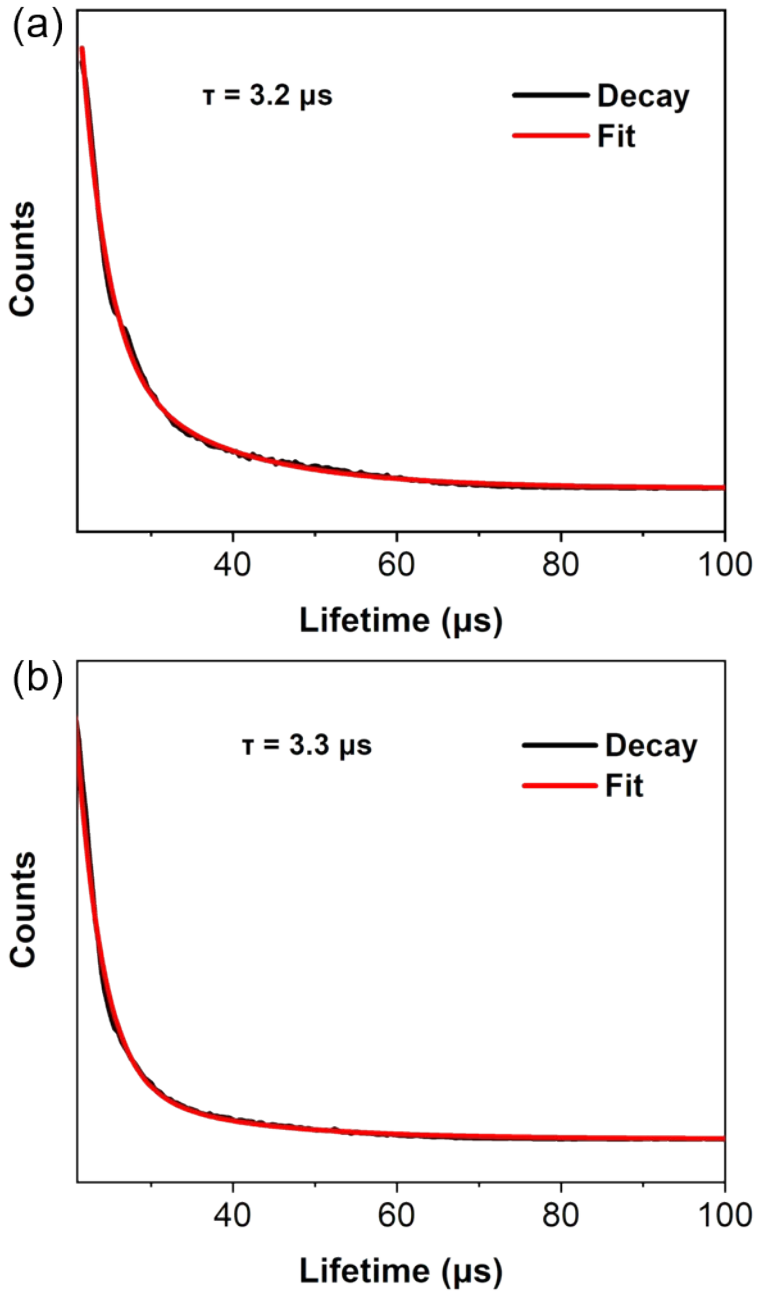

Figure S19. Decay lifetimes of ***R*-Ag$_5$-3** (a) and ***S*-Ag$_5$-3** (b) in solid state.

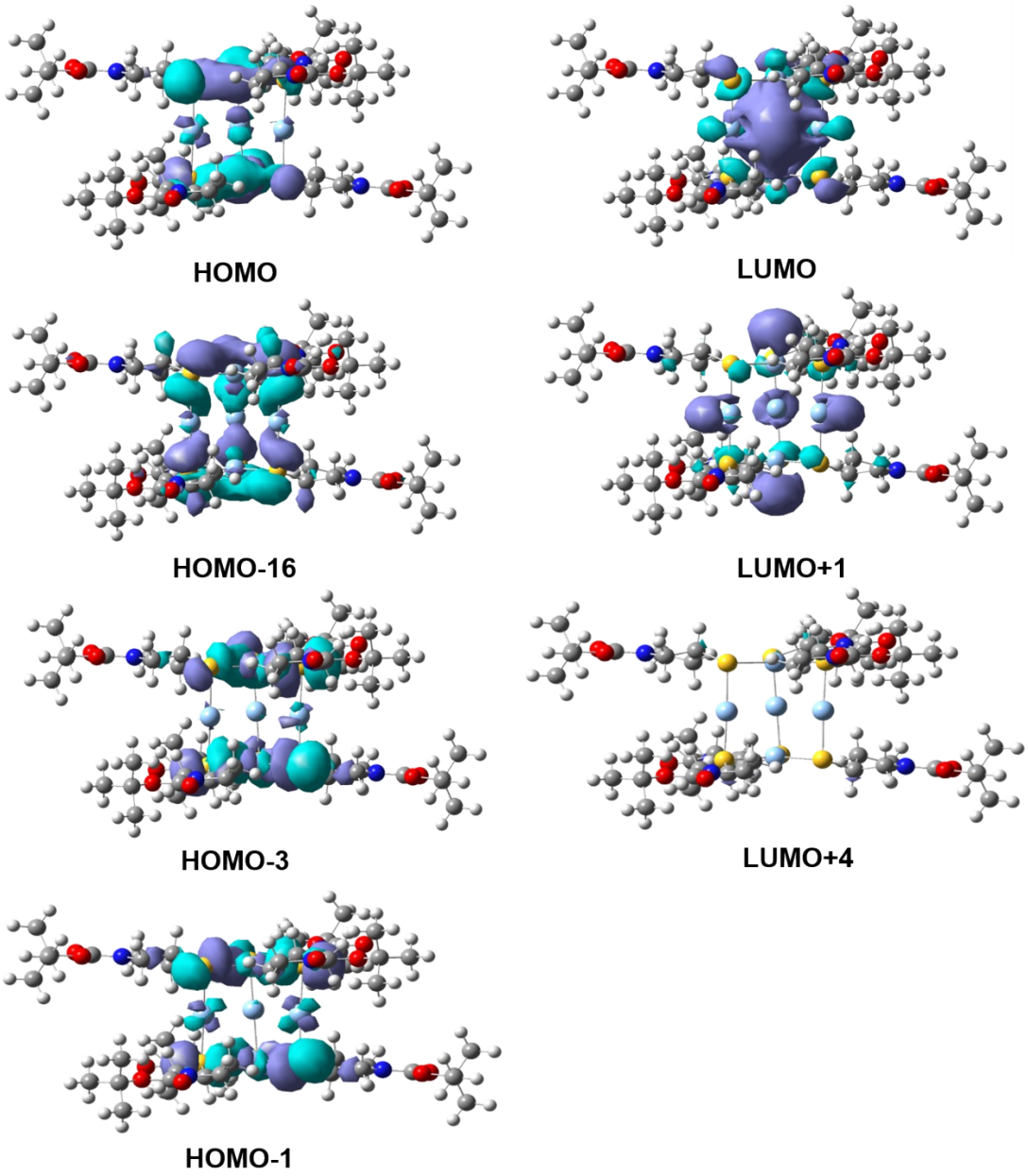

Figure S20. Selected frontier molecular orbitals of ***R*-Ag$_5$-3'**. Hydrogen atoms are omitted for clarity.

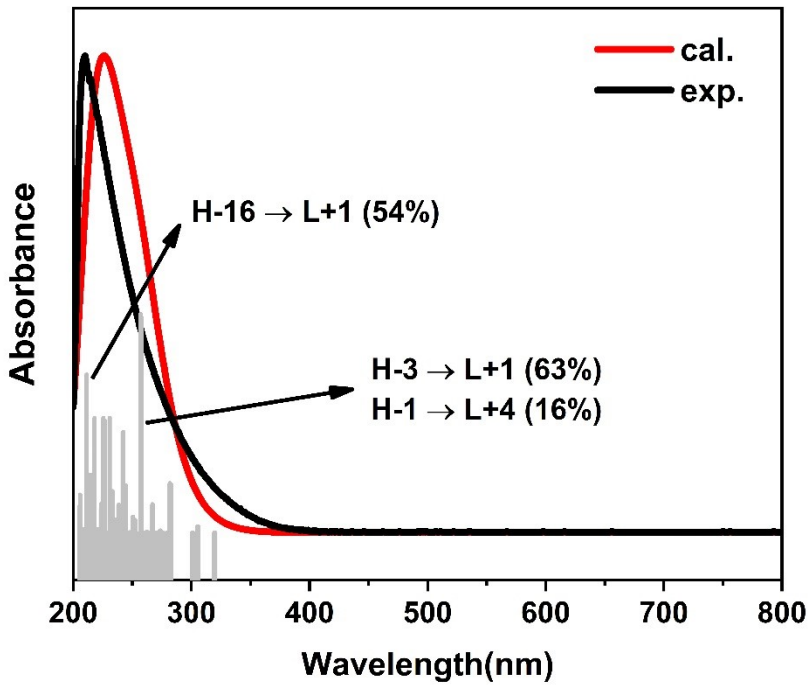

Figure S21. Experimental optical absorption spectrum (black) of ***R*-Ag$_5$-3** in CH_3OH compared to the calculated spectrum (red). Grey bars show the individual transitions (delta-function-like peaks showing the relative oscillator strengths).

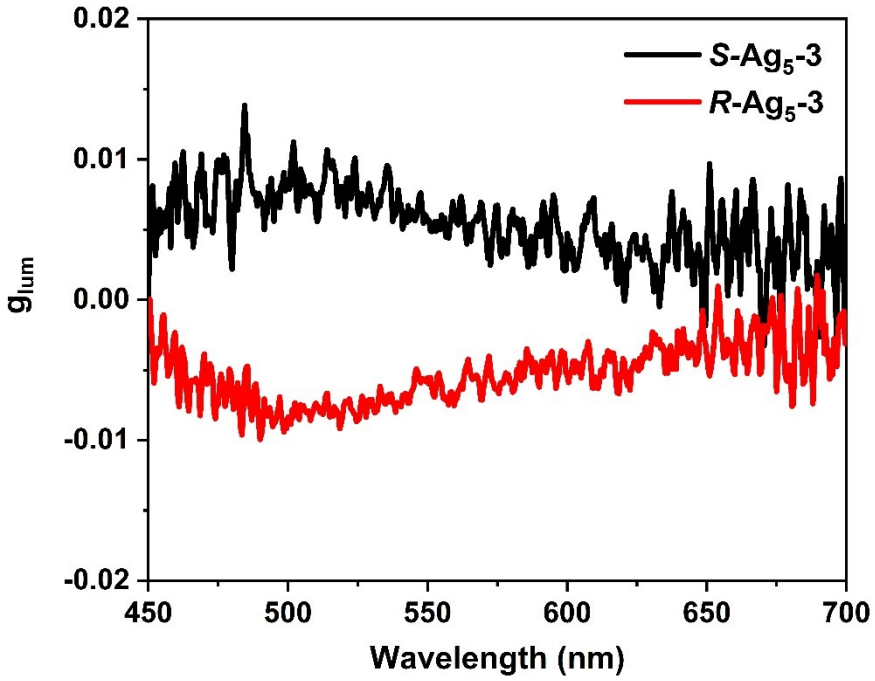

Figure S22. Corresponding g_{lum} values of ***S*-Ag$_5$-3** (black curve) and ***R*-Ag$_5$-3** (red curve) in the solid state.

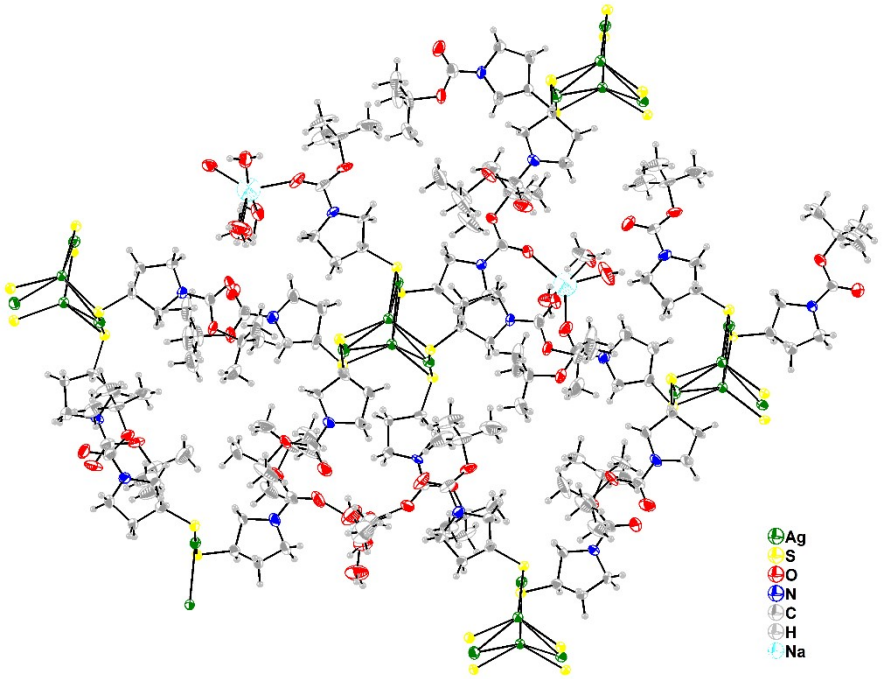

Figure S23. The structure of ***R*-Ag$_5$-1**.

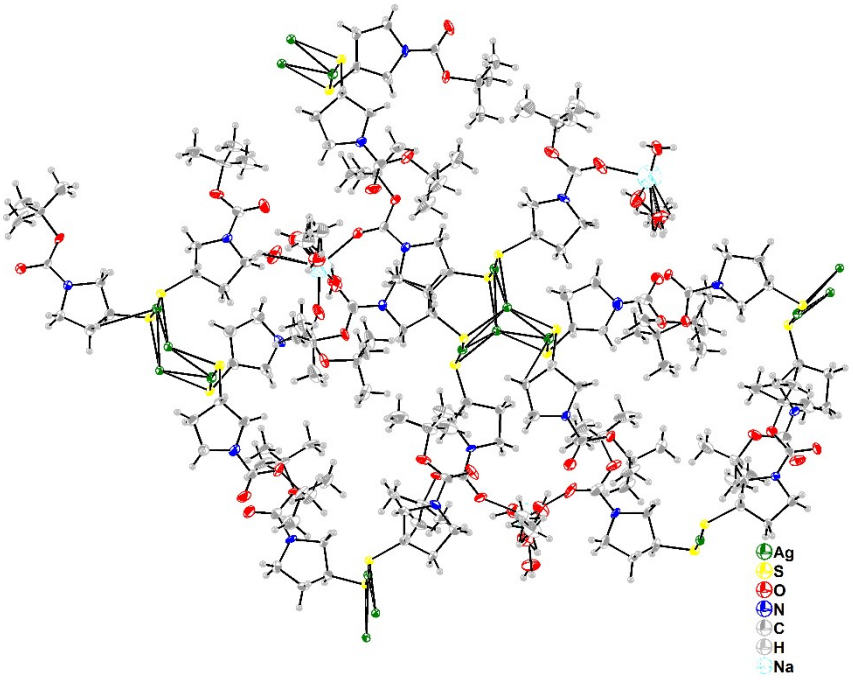

Figure S24. The structure of ***S*-Ag$_5$-1**.

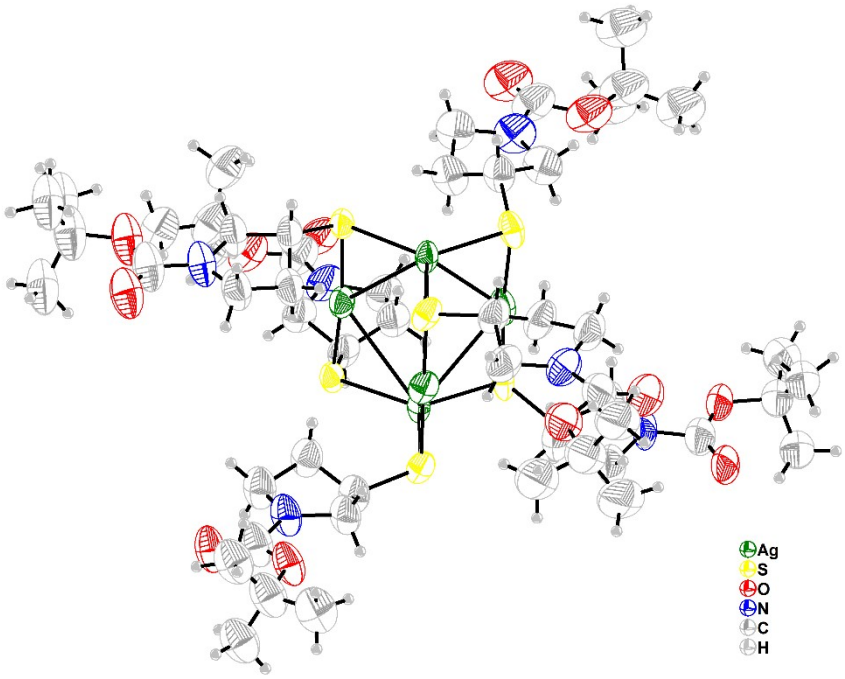

Figure S25. The structure of ***R*-Ag$_5$-2** (200K).

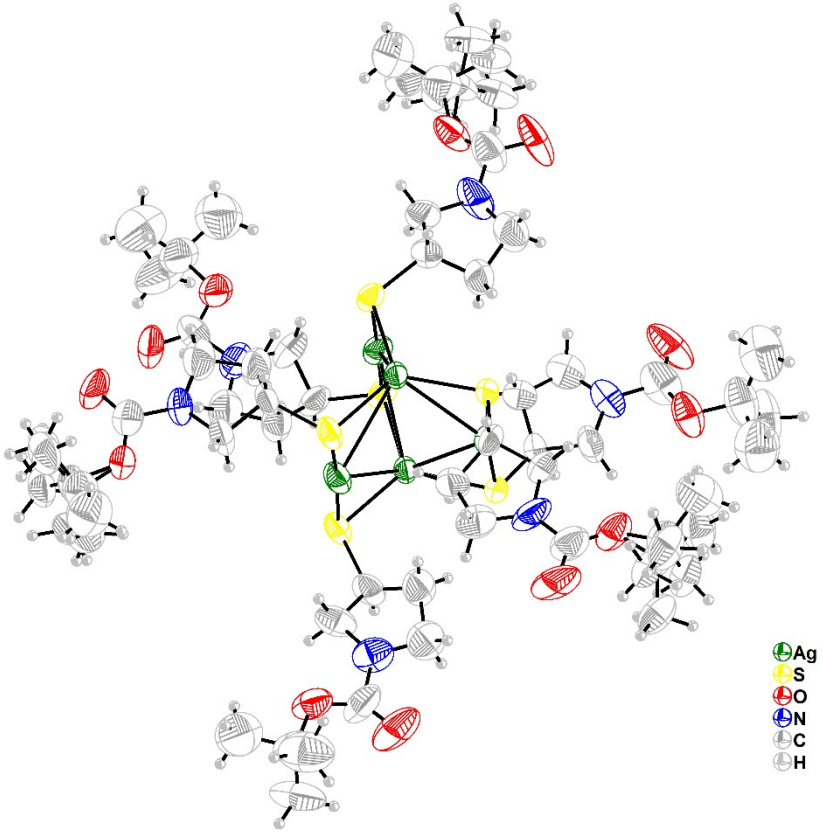

Figure S26. The structure of ***S*-Ag$_5$-2** (200K).

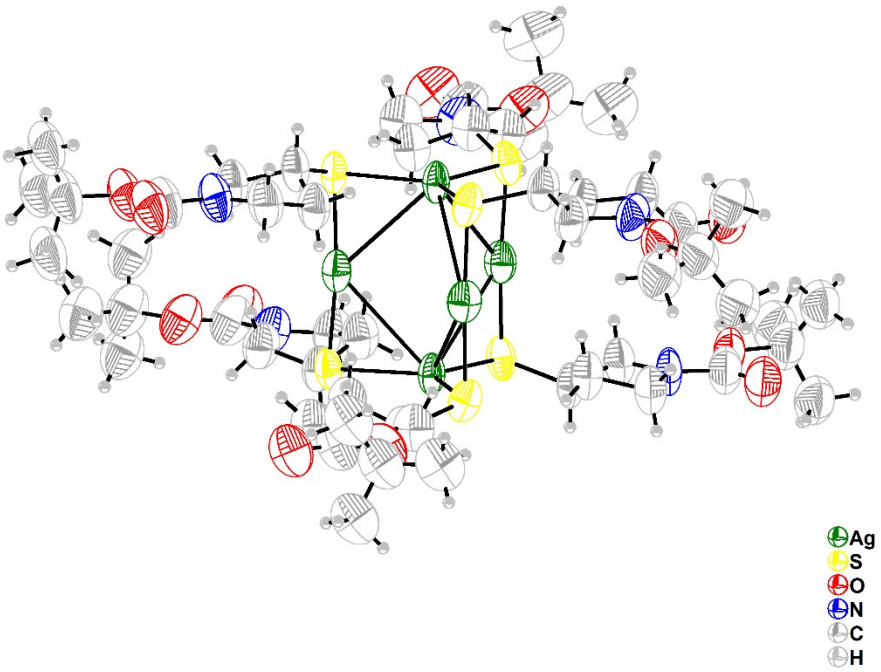

Figure S27. The structure of ***R*-Ag$_5$-2** (295K).

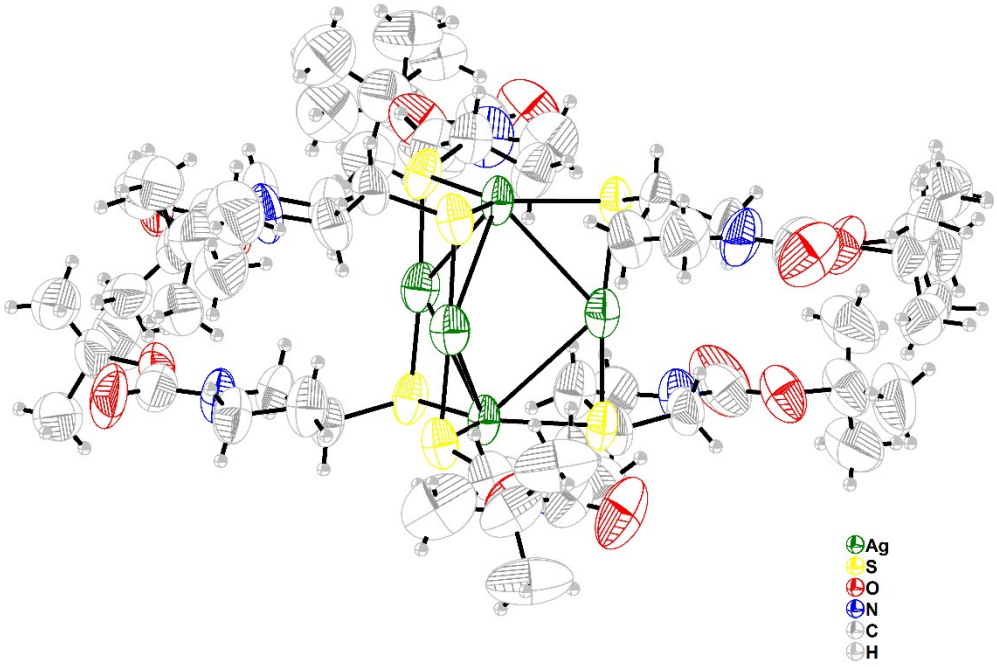

Figure S28. The structure of ***S*-Ag$_5$-2** (295K).

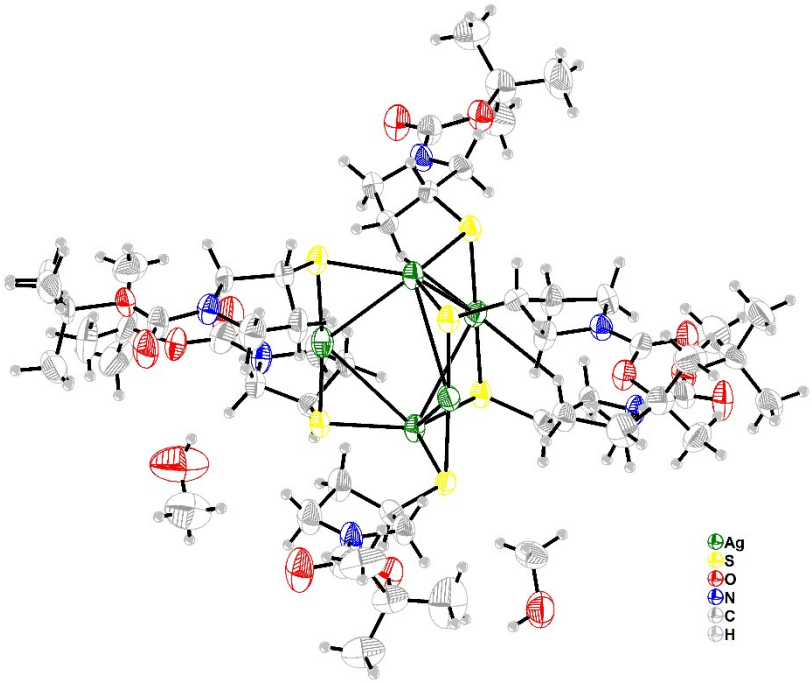

Figure S29. The structure of ***R*-Ag$_5$-3**.

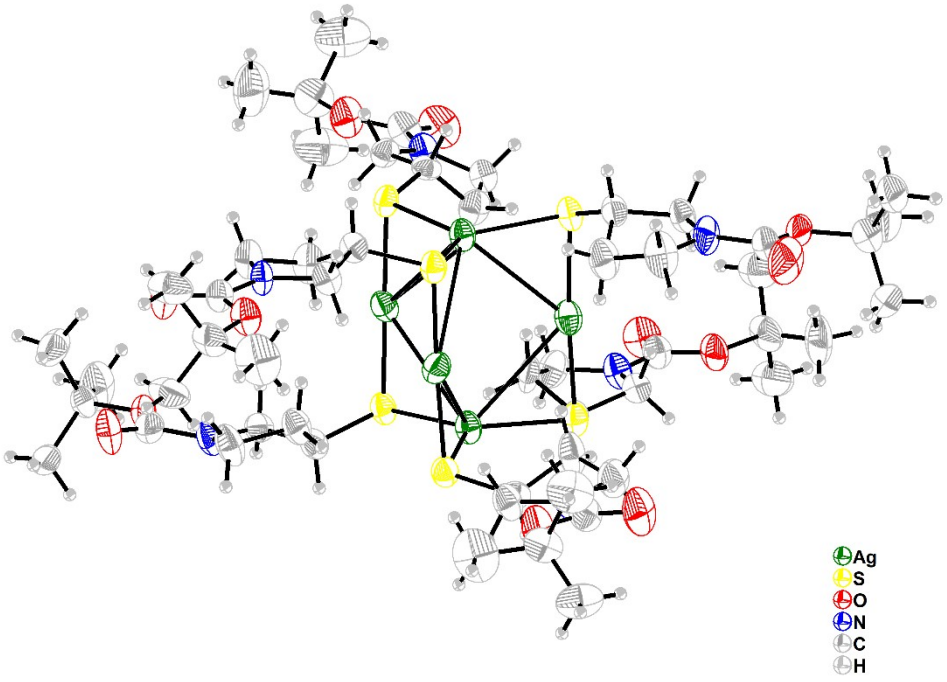

Figure S30. The structure of ***S*-Ag$_5$-3**.

Table S2. Crystal data and structure refinements for *R*-Ag_5-1 and *S*-Ag_5-1 at 200 K.

	***S*-Ag_5-1**	***R*-Ag_5-1**
Empirical formula	$C_{55}H_{104}Ag_5N_6NaO_{15}S_6$	$C_{55}H_{104}Ag_5N_6NaO_{15}S_6$
Formula weight	1844.14	1836.55
Temperature / K	200.00(10)	200.00(10)
Crystal system	trigonal	trigonal
Space group	*P*3	*P*3
a / Å	46.5977(4)	46.6686(2)
b / Å	46.5977(4)	46.6686(2)
c / Å	9.12498(9)	9.21350(10)
α / °	90	90
β / °	90	90
γ / °	120	120
Volume / Å^3	17159.0(3)	17378.2(2)
Z	9	9
ρ_{calc} / g cm^{-3}	1.606	1.579
μ / mm^{-1}	12.198	12.040
F (000)	8442.0	8403.0
Crystal size / mm^3	0.12 × 0.1 × 0.05	0.12 × 0.1 × 0.05
Radiation	CuKα (λ = 1.54184)	CuKα (λ = 1.54184)
2ϑ range for data collection / °	5.794 to 147.638	3.786 to 145.094
Index ranges	-58 ≤ *h* ≤ 57, -55 ≤ *k* ≤ 57, -8 ≤ *l* ≤ 11	-57 ≤ *h* ≤ 56, -56 ≤ *k* ≤ 45, -10 ≤ *l* ≤ 11
Reflections collected	64009	93957
Independent reflections	[R_{int} = 0.0331, R_{sigma} = 0.0630]	[R_{int} = 0.0351, R_{sigma} = 0.0544]
Data / restraints / parameters	29925 / 686 / 2492	41414 / 469 / 2477
Goodness-of-fit on F^2	0.918	0.878
Final *R* indexes [$I >= 2\sigma(I)$]	R_1 = 0.0312, wR_2 = 0.0703	R_1 = 0.0293, wR_2 = 0.0624
Final *R* indexes [all data]	R_1 = 0.0334, wR_2 = 0.0715	R_1 = 0.0318, wR_2 = 0.0637
Flack parameter	-0.009(4)	-0.011(3)
CCDC	2192032	2192034

$R_1 = \sum||F_o|-|F_c||\sum/|F_o|$. $wR_2 = [\sum w(F_o^2 - F_c^2)^2/\sum w(F_o^2)^2]^{1/2}$

Table S3. Crystal data and structure refinements for *R*-Ag_5-2 and *S*-Ag_5-2 at 200 K.

	***S*-Ag_5-2**	***R*-Ag_5-2**
Empirical formula	$C_{54}H_{96}Ag_5N_6O_{12}S_6$	$C_{54}H_{96}Ag_5N_6O_{12}S_6$
Formula weight	1753.09	1753.07
Temperature / K	200.0	200.0
Crystal system	trigonal	trigonal
Space group	*P*3	*P*3
a / Å	15.5807(8)	15.5680(10)
b / Å	15.5807(8)	15.5680(10)
c / Å	9.2970(5)	9.2630(8)
α / °	90	90
β / °	90	90
γ / °	120	120
Volume /Å^3	1954.6(2)	1944.2(3)
Z	0.99999	1
ρ_{calc} g / cm^3	1.489	1.497
μ / mm^{-1}	1.442	1.449
F (000)	889.0	889.0
Crystal size / mm^3	0.07 × 0.06 × 0.05	0.11 × 0.1 × 0.06
Radiation	MoKα (λ = 0.71073)	MoKα (λ = 0.71073)
2ϑ range for data collection / °	5.322 to 54.874	5.336 to 55.41
Index ranges	-20 ≤ *h* ≤ 20, -20 ≤ *k* ≤ 20, -11 ≤ *l* ≤ 11	-20 ≤ *h* ≤ 20, -20 ≤ *k* ≤ 20, -11 ≤ *l* ≤ 12
Reflections collected	77333	98840
Independent reflections	[R_{int} = 0.0607, R_{sigma} = 0.0232]	[R_{int} = 0.0864, R_{sigma} = 0.0310]
Data / restraints / parameters	5923 / 191 / 293	5993 / 485 / 257
Goodness-of-fit on F^2	1.054	1.034
Final *R* indexes [$I >= 2\sigma(I)$]	R_1 = 0.0511, wR_2 = 0.1410	R_1 = 0.0503, wR_2 = 0.1303
Final *R* indexes [all data]	R_1 = 0.0606, wR_2 = 0.1509	R_1 = 0.0631, wR_2 = 0.1412
Flack parameter	0.004(13)	0.008(18)
CCDC	2192035	2192036

$R_1 = \sum||F_o|-|F_c||\sum/|F_o|$. $wR_2 = [\sum w(F_o^2 - F_c^2)^2/\sum w(F_o^2)^2]^{1/2}$

Table S4. Crystal data and structure refinements for *R*-Ag_5-2 and *S*-Ag_5-2 at 295 K.

	***S*-Ag_5-2**	***R*-Ag_5-2**
Empirical formula	$C_{54}H_{96}Ag_5N_6O_{12}S_6$	$C_{54}H_{96}Ag_5N_6O_{12}S_6$
Formula weight	1753.09	1753.07
Temperature / K	295.0	296.0
Crystal system	trigonal	trigonal
Space group	*P*3	*P*3
a / Å	15.5807(8)	15.5680(10)
b / Å	15.5807(8)	15.5680(10)
c / Å	9.2970(5)	9.2630(8)
α / °	90	90
β / °	90	90
γ / °	120	120
Volume /Å^3	1954.6(2)	1944.2(3)
Z	0.99999	1
ρ_{calc} g / cm^3	1.489	1.497
μ / mm^{-1}	1.442	1.449
F (000)	889.0	889.0
Crystal size / mm^3	0.07 × 0.06 × 0.05	0.11 × 0.1 × 0.06
Radiation	MoKα (λ = 0.71073)	MoKα (λ = 0.71073)
2ϑ range for data collection / °	4.382 to 54.962	5.336 to 55.21
Index ranges	-20 ≤ *h* ≤ 20, -20 ≤ *k* ≤ 20, -12 ≤ *l* ≤ 12	-20 ≤ *h* ≤ 20, -20 ≤ *k* ≤ 20, -12 ≤ *l* ≤ 12
Reflections collected	133770	50366
Independent reflections	[R_{int} = 0.0537, R_{sigma} = 0.0154]	[R_{int} = 0.0457, R_{sigma} = 0.0258]
Data / restraints / parameters	6012 / 156 / 295	5991 / 497 / 257
Goodness-of-fit on F^2	1.041	1.088
Final *R* indexes [$I >= 2\sigma(I)$]	R_1 = 0.0446, wR_2 = 0.1276	R_1 = 0.0532, wR_2 = 0.1417
Final *R* indexes [all data]	R_1 = 0.0548, wR_2 = 0.1358	R_1 = 0.0604, wR_2 = 0.1470
Flack parameter	0.018(8)	0.79/-0.58
CCDC	2192037	2192033

$R_1 = \sum||F_o|-|F_c||\sum/|F_o|$. $wR_2 = [\sum w(F_o^2 - F_c^2)^2/\sum w(F_o^2)^2]^{1/2}$

Table S5. Crystal data and structure refinements for *R*-Ag_5-3' and *S*-Ag_5-3' at 200 K.

	***S*-Ag_5-3'**	***R*-Ag_5-3'**
Empirical formula	$C_{54}H_{96}Ag_5N_6O_{12}S_6$	$C_{54}H_{96}Ag_5N_6O_{12}S_6$
Formula weight	1753.07	1817.16
Temperature / K	199.99(10)	200.00(10)
Crystal system	triclinic	triclinic
Space group	*P*1	*P*1
a / Å	10.4215(7)	10.5113(7)
b / Å	13.7248(6)	13.7344(12)
c / Å	15.1755(8)	15.1850(14)
α / °	64.698(5)	64.591(9)
β / °	71.721(5)	71.808(7)
γ / °	78.236(4)	78.249(7)
Volume /Å^3	1857.2(2)	1875.0(3)
Z	1	1
ρ_{calc} g / cm^3	1.567	1.609
μ / mm^{-1}	12.407	12.332
F (000)	889.0	925.0
Crystal size / mm^3	0.1 × 0.1 × 0.05	0.1 × 0.1 × 0.05
Radiation	CuK*α* (*λ* = 1.54184)	CuK*α* (*λ* = 1.54184)
2*ϑ* range for data collection / °	6.664 to 148.854	6.664 to 147.258
Index ranges	-12 ≤ *h* ≤ 12, -15 ≤ *k* ≤ 17, -12 ≤ *l* ≤ 18	-11 ≤ *h* ≤ 13, -16 ≤ *k* ≤ 17, -18 ≤ *l* ≤ 16
Reflections collected	18436	17473
Independent reflections	[R_{int} = 0.0625, R_{sigma} = 0.0741]	[R_{int} = 0.0536, R_{sigma} = 0.0662]
Data / restraints / parameters	9052 / 3 / 766	9231 / 17 / 806
Goodness-of-fit on F^2	1.019	1.081
Final *R* indexes [$I >= 2\sigma(I)$]	R_1 = 0.0747, wR_2 = 0.1965	R_1 = 0.0596, wR_2 = 0.1557
Final *R* indexes [all data]	R_1 = 0.0789, wR_2 = 0.2029	R_1 = 0.0648, wR_2 = 0.1601
Flack parameter	-0.003(17)	-0.023(12)
CCDC	2192030	2192031

$R_1 = \sum||F_o|-|F_c||\sum/|F_o|$. $wR_2 = [\sum w(F_o^2 - F_c^2)^2/\sum w(F_o^2)^2]^{1/2}$

Reference

[1] CrysAlisPro, Version 1.171.36.31, Software for Crystal Data Collection and Reduction, Agilent technologies Inc., Santa Clara, CA, USA, 2012.

[2] CrysAlisPro 1.171.38.41k (Rigaku Oxford Diffraction, 2015).

[3] G. M. Sheldrick, A short history of SHELX, *Acta Cryst. A*, 2008, **64**, 112-122.

[4] O. V. Dolomanov, L. J. Bourhis, R. J. Gildea, J. A. Howard, H. Puschmann, OLEX2: a Complete Structure Solution, Refinement and Analysis Program, *J. Appl. Cryst.*, 2009, **42**, 339-341.

[5] G. Sheldrick, Crystal Structure Refinement with SHELXL, *Acta Cryst. C*, 2015, **71**, 3-8.

[6] M. J. Frisch, Gaussian, Inc., Wallingford CT, 2016.

[7] J. P. Perdew, K. Burke, M. Ernzerhof, Generalized Gradient Approximation Made Simple, *Phys. Rev. Lett.*, 1996, **77**, 3865-3868.

[8] G. A. Petersson, A. Bennett, T. G. Tensfeldt, M. A. Al-Laham, W. A. Shirley, J. Mantzaris, A complete basis set model chemistry. I. The total energies of closed-shell atoms and hydrides of the first-row elements, *J. Chem. Phys.*, 1988, **89**, 2193-2218.

[9] G. A. Petersson, M. A. Al-Laham, A complete basis set model chemistry. II. Open-shell systems and the total energies of the first-row atoms, *J. Chem. Phys.*, 1991, **94**, 6081-6090.

[10] P. Fuentealba, H. Preuss, H. Stoll, L. V. Szentpály, A proper account of core-polarization with pseudopotentials: single valence-electron alkali compounds, *Chem. Phys. Lett.*, 1982, **89**,418-422.

[11] N. M. O'Boyle, A. L. Tenderholt, K. M. Langner, cclib: A library for package-independent computational chemistry algorithms, *J. Comput. Chem.*, 2008, **29**, 839-845.

[12] T. Lu, F. W. Chen, Multiwfn: A multifunctional wavefunction analyzer, *J. Comput. Chem.*, 2012, **33**, 580-592.